HIGH-POWER THIRD-HARMONIC FLAT LASER PULSE GENERATION

C. Vicario *(INFN/LNF)*, M. Petrarca. *(INFN/Roma1)*, S. Cialdi *(INFN/Milano)* P. Musumeci *(UCLA)*.

Abstract

The generation of a high-power laser pulse at 266 nm that is longitudinally shaped according to a prefixed intensity profile is reported. The main features of the pulse shape modifications due to second- and third harmonic conversions are measured, and the results are in good agreement with the theory. The UV temporal shape depends on the chirp of the fundamental pulse and on the crystal phase-matching angle. Exploiting the large stretching imposed on the third-harmonic signal, we show that the pulse intensity profile can be obtained by spectral single-shot measurements.

1   INTRODUCTION

The generation of high energy laser pulses with a few picoseconds time width, center wavelength at 266 *nm*, flat top temporal profile with fast rise and fall time, is of great interest for the photoemission from metal cathodes of electron bunches characterized by low emittance (*about* 1 *mm−mrad*) and high current [1–3]. In this report we present some pulse shape measurements going through the evolution from the fundamental towards the third harmonic generation and we show how to do to obtain the target pulse shape. We also demonstrate that the pulse intensity profile can be obtained directly by spectral measurements. In the following we first describe our laser system, then we discuss the experimental results and the theory.
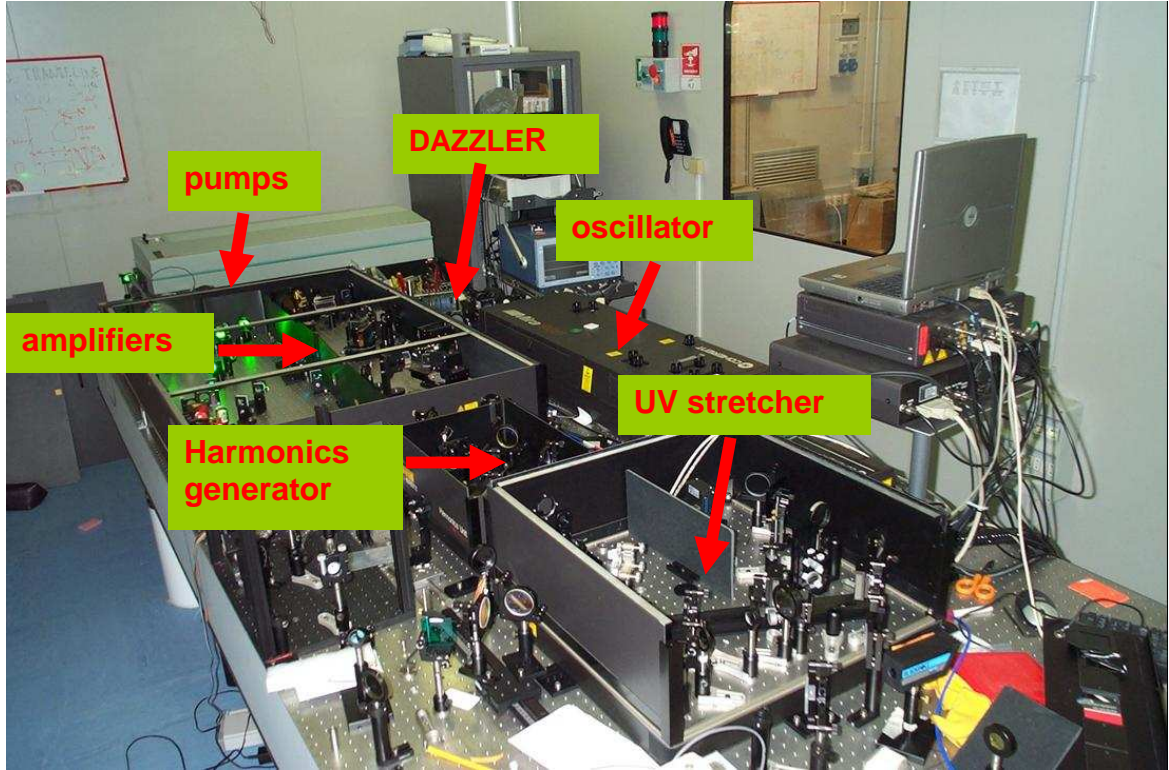

Figure 1. SPARC laser system

We refer to the SPARC, reported in Fig.1 laser system that is based on a Ti:Sa oscillator that generates 100 *fs* pulses with a repetition rate of 79+1/3 MHz. An acousto-optic programmable dispersive filter called "DAZZLER," [4] used to modify the spectral amplitude and phase function, is placed between the oscillator and the amplifier to obtain the target temporal profile[5]. The picture of the DAZZLER set up is reported in Fig. 2. The amplification process is carried out by one regenerative pre-amplifier pumped by 10 W frequency doubled Nd:YLF laser and a two double passes stages which are excited by the second harmonic of a Nd:YAG with an energy of 0.5 J per pulse. The system delivers pulses at λ=800 nm with energy of about 50 mJ and a repetition rate of 10 Hz.

Figure 2. Dazzler set-up: the oscillator output is sent to the acousto-optic filter and a half wavelength wave-plate. After, a periscope is used to inject the beam in the amplifier.

At the output of the amplifier the IR pulses go to a third harmonic generator, where UV pulses with an energy of up to 4 mJ are produced. The up-conversion is required to generate photon with energy larger than the photoemission work function of the metal cathode. The third harmonic generator is characterized by two type I beta barium borate (BBO) crystals of 0.5 and 0.3 μm used to produce first the second harmonic signal and then the third harmonic signal by frequency sum. The third harmonic generator is shown in Fig. 3 and Fig 4.

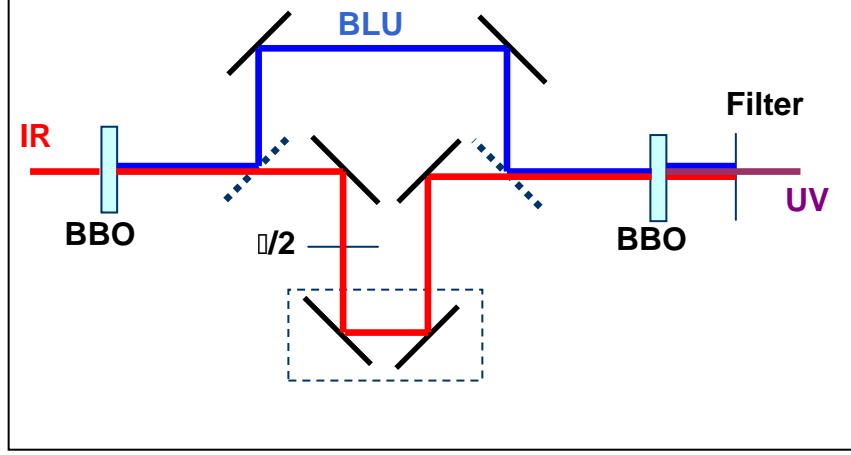Figure 3 Picture of the third harmonic generator.

Figure 4 Sketch of the third harmonic generator.

At the end of the laser chain there is a grating stretcher based on a pair of 4350 groove/mm UV reflecting gratings that is used to stretch the pulses temporally by up to 8–12 ps. In this way the IR pulse length at the entrance of the third harmonic generator does not change and therefore the harmonic conversion efficiency is independent on the laser pulse length desired on the cathode.

2   TEMPORAL PULSE SHAPE THROUGH THE HARMONIC GENERATION

We present the theory that take into account the distortion introduced by the harmonic generation process and technique we employed to produce a quasi-square pulse in the third harmonic at high-energy level [5]. Our procedure is based on the DAZZLER, which provides the proper phase and amplitude modulation to obtain the target third harmonic spectrum profile that corresponds to the wanted time profile.
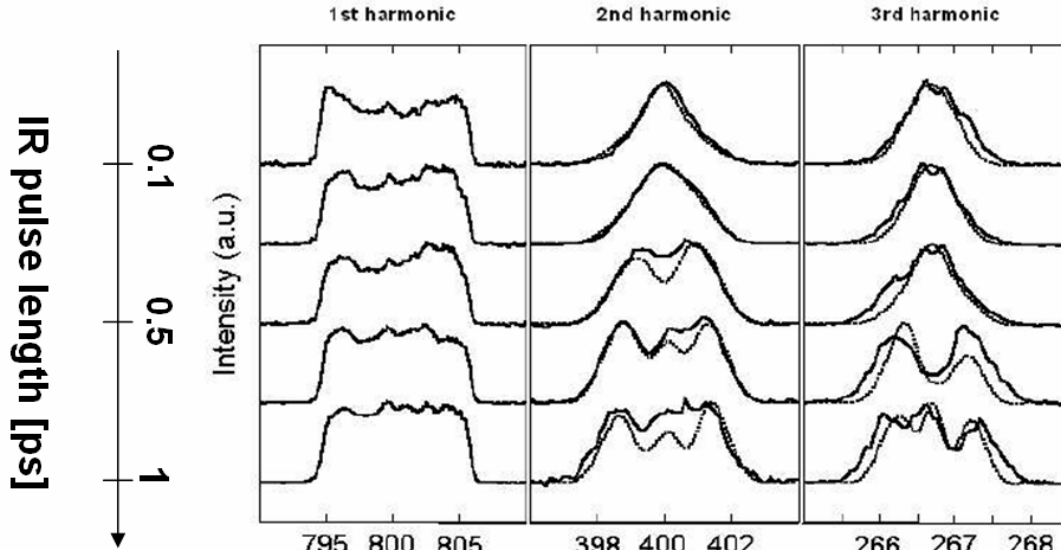

Fig. 5. From left to right: measured (solid curve) and simulated (dashed curve) IR, BLUE, and UV spectra. Starting from a transform-limited pulse, we increase the chirp by 0.01 ps^2 for each curve from top to bottom.

As reported in Ref. 6, the target temporal pulse is obtained by generating a UV rectangular spectrum and then converting it into a rectangular temporal shape by the stretcher. As said, it is not possible to produce a 10 ps rectangular pulse before the harmonic generation chain because otherwise the conversion efficiency of the two BBO crystals would be too low. At the same time it is important to stress that it is not possible for the IR laser pulses to enter the crystals with temporal pulses that are too short. In fact, the generated second harmonic and third harmonic spectral widths depend strongly on the first-harmonic pulse length.[7] This behavior is shown in Fig. 5 by reporting the changes that occur in the spectrum of the second harmonic and third harmonic signals as a function of the chirp introduced by the DAZZLER. In the left part of the figure the first-harmonic spectra shaped by the DAZZLER are presented; the middle and the right parts show the experimental and calculated second harmonic and third harmonic spectra, respectively. Starting from a transform-limited pulse, we increase the chirp by 0.01 ps^2 for each curve from top to the bottom. As shown in the figure there are a good agreement between the measured spectra and the simulated ones.

As a consequence the pulse length increases from roughly 100 fs to about1 ps. As shown in the figure, when the first-harmonic pulse is transform limited, the second harmonic and third harmonic spectra have a narrow bell shape. When the chirp is increased, the second harmonic and third harmonic spectral shapes become quasi-rectangular. The theory of this behavior has been settled in Ref. 7 and is briefly reported in the following. Let us consider the general case of pulse generation with central frequency ω_3 from the interaction in a nonlinear crystal of two pulses with central frequencies ω_1 and ω_2, where $\omega_3=\omega_1+\omega_2$. Moreover, pulse generation under a non-depletion condition [8,9] is assumed, and the dispersion factor is neglected due to the short crystal length of 300 μm. For complex amplitude A_3 the following equation holds:

$$\frac{\partial A_3}{\partial z} + \frac{1}{V_{g3}}\frac{\partial A_3}{\partial t} = i\gamma A_1 A_2 e^{-i\Delta kz} \tag{1}$$

where V_{g3} is the group velocity of the pulse at frequency $_3$, is a phenomenological constant taking into account the effective nonlinear coefficient of the crystal, and $\Delta k=k_3-k_2-k_1$ is the imbalance of momentum conservation [8]. Since we are in the non-depletion regime, pulses A_1 and A_2 are not appreciably modified while propagating along the crystal. They propagate with velocities V_{g1} and V_{g2}, respectively; therefore $A_1=A_1[(t-z)/V_{g1}]$ and $A_2=A_2[(t-z)/V_{g2}]$. Substituting these expressions into Eq. (1), applying the time transformation $t_1=t-z/V_{g3}$, and making a Fourier transform, we obtain

$$\frac{\partial \tilde{A}_3}{\partial z} = i\gamma \left[\left(\tilde{A}_1 e^{-i\beta_{31}z\omega} \right) \otimes \left(\tilde{A}_2 e^{-i\beta_{32}z\omega} \right) \right] e^{-i\Delta kz} \tag{2}$$

where $\beta_{ij}=1/V_{gi}-1/V_{gj}$. In the following all the simulated curves are calculated as a numerical solution of Eq. (2). Consider, for example, type I second harmonic generation in the case of perfect phase matching. In this situation we have $\beta_{31}=\beta_{32}=\beta$, thus we achieve:

$$\partial \tilde{A}_3/\partial z = i\gamma[\tilde{A}_1 \otimes \tilde{A}_1]\exp(-i\beta z\omega). \tag{3}$$

Therefore, considering rectangular spectra in the fundamental harmonic, the convolution yields a triangular spectrum shape for the second harmonic. Thus transform-limited pulses do not give a rectangular spectrum in the second harmonic. On the contrary, by introducing a chirp into the fundamental signal, the initial rectangular shape can be preserved. In fact, considering $\hat{A}_1(\omega) = S(\omega)exp[i\Phi(\omega)]$ with $S(\omega)$ real and $\Phi(\omega)=\alpha\omega^2/2$, where α is the chirp strength introduced by the DAZZLER, we obtain:

$$\tilde{A}_1 \otimes \tilde{A}_1(\omega) = \int S(\omega - \Omega)S(\Omega)e^{i(\phi(\omega-\Omega)+\phi(\Omega))}d\Omega \qquad (4)$$

Since in the phase factor, $\Phi(\omega-\Omega)+\Phi(\omega)$ is a parabolic function centered at $\Omega=\omega/2$, the dominant contribution comes for Ω close to $\omega/2$ when enough chirp is applied. Thus we can write:

$$\tilde{A}_1 \otimes \tilde{A}_1(\omega) \sim S^2(\omega/2)e^{2\phi(\omega/2)} \qquad (5)$$

Therefore increasing the chirp in the fundamental beam, the leading behavior of the second harmonic spectral intensity is given by the square of the fundamental with twice the spectral width and the second harmonic spectrum changes its from triangular shape to rectangular one. Moreover, being the second harmonic spectrum proportional to the square of the initial one, the increasing of the ripple in the higher harmonic is explained too. The above considerations can be extended to the third harmonic generation. The results of this discussion are that it is necessary to introduce a large enough chirp factor on the 800nm pulse in order to produce a UV rectangular spectrum. The amount of this chirp has to be determined accurately because a large value can reduce to much the conversion efficiency.
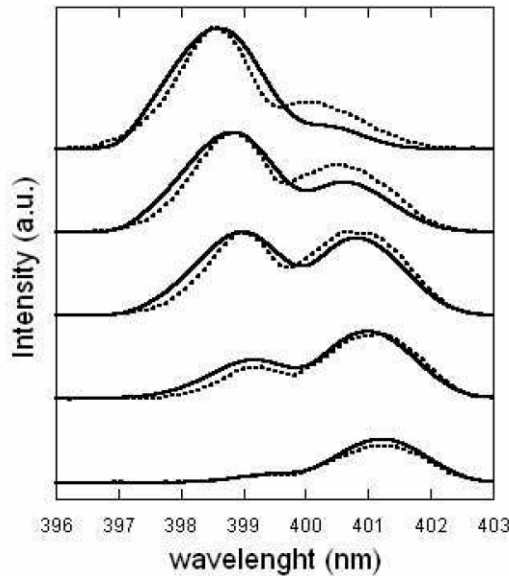

Fig. 6. SH simulated (solid curve) and measured (dashed curve) spectrum changes versus the tilt of the crystal from its phase-matching angle. The tilt from top to bottom is 5.8, 2.9, 0, −2.9, and −5.8 mrad.

Changing the crystal phase matching angle, the spectral shape of the harmonic signal generated as well as its efficiency strongly changes. In fact, as it is shown in Fig. (6), flipping by few mrad the crystal angle, the second harmonic spectrum is modulated asymmetrically. To explain this behavior, let us consider Eq. (2). Since we are concerning the second harmonic generation process, we can replace $\beta_{31} = \beta_{32} = \beta$ and assume in first approximation $\Delta k = \chi \theta$ where the parameter χ depends on the crystal type and θ is the angular displacement from the phase matching condition. The following equation is archived:

$$\frac{\partial \tilde{A}_3}{\partial z} = i\gamma \left[\tilde{A}_1 \otimes \tilde{A}_1 \right] e^{-i\beta(\omega + \frac{\chi}{\beta}\theta)z} \tag{6}$$

Integrating this equation over the crystal length d and calculating the intensity we get:

$$\tilde{I}_3 \propto sinc^2 \left(\beta(\omega + \frac{\chi}{\beta}\theta)d \right) d^2 \left| \left[\tilde{A}_1 \otimes \tilde{A}_1 \right] \right|^2 \tag{7}$$

It is clear that changing θ we move the center of the sinc function with respect to the convolution product. This can produce an enhancement of the lower or upper second harmonic spectral components depending on the sign of θ. In our case we used a BBO crystal which has a relatively high value for the χ parameter, such that small changes of few mrad for the angle θ are enough to produce large spectrum distortion.

It is important the fine alignment of the harmonic crystals. In fact, not only the harmonic efficiency conversion but also the spectrum profile and therefore the time domain intensity are strongly influenced by the phase-matching angle.

Now we want to show that it is possible to construct a pulse with an arbitrary intensity spectrum shape, and that the pulses produced have a temporal profile out of the UV stretcher that is well approximated by its power spectrum [6]. This is achieved by introducing enough temporal linear chirp troughs the UV stretcher.
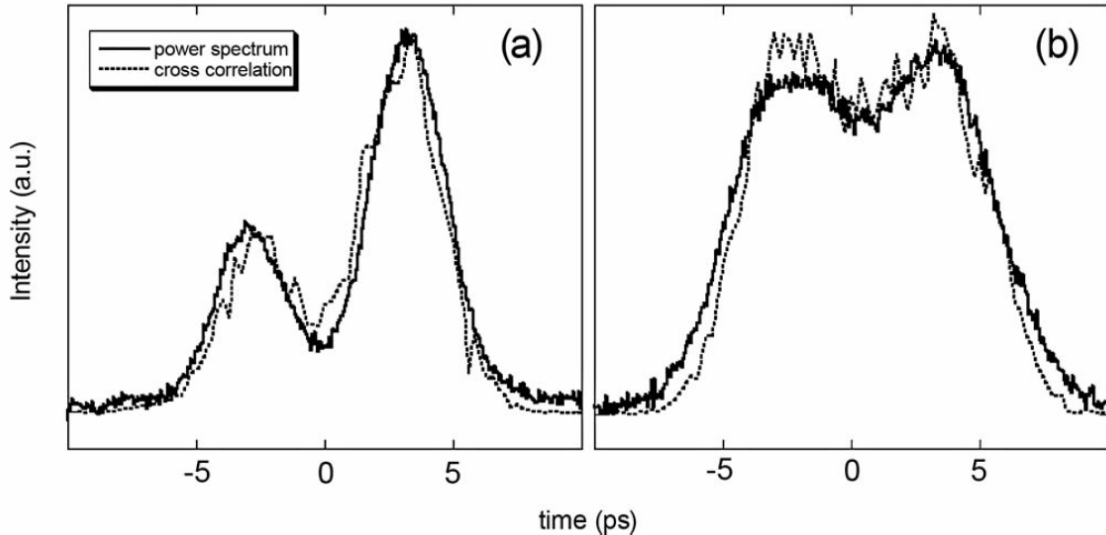

Fig. 7. Comparison between the UV spectrum (solid curve) and the temporal profile (dashed curve) after the UV stretcher in two cases.

In Fig. (7) two examples are shown: we compare the spectral profile, solid line, and the time profile, dashed line. The correlation between spectrum and time intensity has been studied and experimentally confirmed using two home-built diagnostic tools: a spectrometer and an UV cross-correlator.

As shown in the Fig. 7 in both cases we obtained a good superposition between the spectrum and the temporal profile. These two profiles, have been produced by introducing with the DAZZLER a proper phase and amplitude modulations in the fundamental. In Fig. (7), the spectral x-axis has been converted in the time coordinate using the relation $\Delta t = a \cdot \Delta \omega$ (in our case $a = 0.3$ ps^2) between angular frequencies and time delay. In these two cases we have a strong pulse stretching, in fact the UV pulse length before the stretcher is about 300 fs while the pulse length after is about 10 ps. The temporal profile has been traced by a UV-IR cross correlator that has been built, studied and characterized by us [10]. As shown a pulse with quite flat plateau can be obtained but the minimum rise time of 2.5 ps is far from the requests.

For completeness we report here the relation between the time profile and its spectrum. Let us consider a pulse with complex amplitude $\hat{A}(\omega)$ and a quadratic phase function given by exp $[i \cdot a \, \omega^2/2]$; the a parameter takes into account the chirp. The time intensity profile, given by the square modulus of the inverse Fourier transform, turns out to be:

$$I(t) = \left| \int \tilde{A}(\omega) \exp\left[i\left(\frac{a\omega^2}{2} - \omega t \right) \right] \mathrm{d}\omega \right|^2 \sim \tilde{I}(\omega = t/a) \tag{8}$$

where $I(\omega) = |\hat{A}(\omega)|^2$ is the power spectrum. In fact, since the phase function is a parabola centered at $\omega = t/a$, the leading contribution to the integral comes from the angular frequencies near the minimum of the phase (for more detail, see Ref. 6). This approximation is true when a large chirp is applied in the third harmonic as for our UV stretcher system. The direct correspondence between the spectrum and the time profile has an important consequence: the spectral profile of the third harmonic can be used as a single-shot time profile diagnostic. This allows circumventing the inherent difficulties to quick measure UV pulses in ps range with an acceptable resolution.

3   MODIFIED STRETCHER TO IMPROVE THE RISE TIME

The measured pulses, and the simulations show limitations on the minimum rise time that can be obtained. As shown in fig 7 the rise time is about 2.5 ps, and the ripple is within 20 % ptp. In fact, due to the finite bandwidth of the non-linear crystals, the steepness of the rise and fall time of the resulting flat-top pulses can not be pre-compensated by the DAZZLER.

The correspondence between spectral and temporal pulse profiles suggests that to improve the rise time the spectral tail has to be sharply clipped. In Fig. 8 in the upper plot, it is reported how the rise time is improved when the spectrum is clipped lower curves. Starting from the black spectrum we remove the tails increasing the steepness of the curve. As shown in the time profile the rise time can be reduced down to 1.2 ps (green curve). At this point sharper cut in the spectrum induce larger ripples but don't improve the rise time due to the given bandwidth.
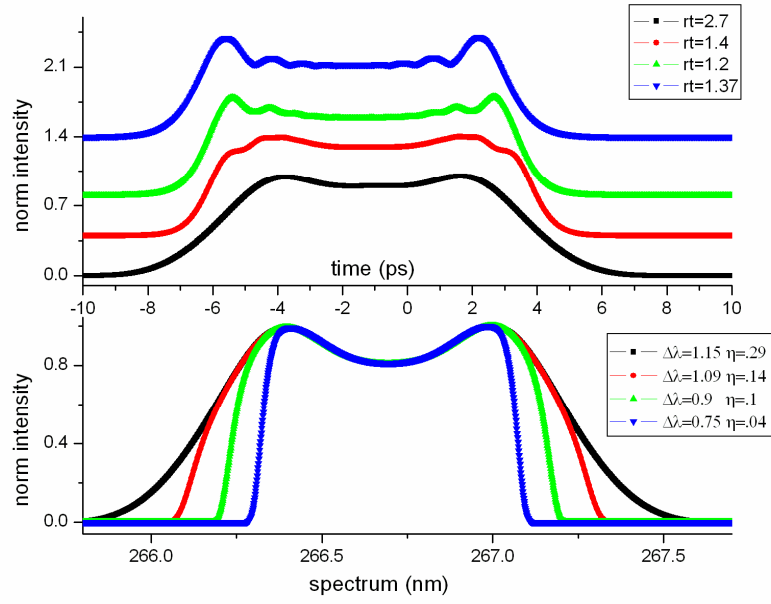
Fig. 8. Effect of the clip of the spectral tails. In the lower plot are reported different spectra obtained by increasing the steepness of the spectra and the correspondent time intensity profile.

To clip the tails of the spectrum we modified the UV stretcher to obtain in a plane a direct correlation between the spectral components and the transverse position. The apparatus is reported in Fig. 9.
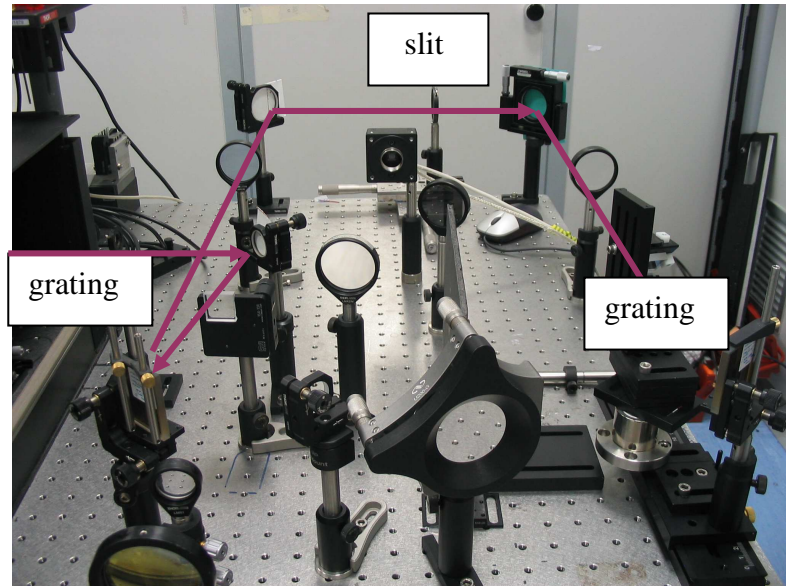

Fig. 9. Modified UV stretcher to implement an UV pulse shape.

Basically the modified stretcher is a particular version of the classical *4f* optical scheme with two anti-parallel gratings and two lenses of focal distance *f* respectively separated by a distance *f* [11]. A collimated beam is sent onto the diffraction grating and it is angularly dispersed horizontally. The pulse wavelenghts are then focused using a positive lens. On the lens focal plane each spectral component will reach a focus in a different position. In other words on this plane there is full correlation between wavelength and transverse position. This allows the cut of the spectral tails simply placing an iris at this plane. The beam is then re-collimated by a second lens and sent to another grating which compared to a classical *4f* system is shifted from the symmetry position (which would be at a distance *f* from the second lens) by a distance *h*. The shift *h* introduces a chirp on the outgoing beam and changes the output pulse length, over the same range of the original version of the UV stretcher.

Using this optical set-up we observed a net improvement on the rise time. We report in fig 10 the cross-correlation measurement on the pulse produced clipping the tails of the spectrum with the described apparatus. The pulse length is about 10 ps FWHM and the rise time is about 1.8 ps. The cross-correlation has been measured using a relatively long IR gate pulse of about 0.6 ps FWHM. The long pulse induces a smoothing in the pulse reconstruction and produces an overestimation on the rise time. According to our calculation the achieved rise time is 1.5 ps. The black curve is obtained using by simulating the real output profile and the calculating the cross correlation with the IR pulse we used. As shown there is a excellent agreement between simulation and measurement.
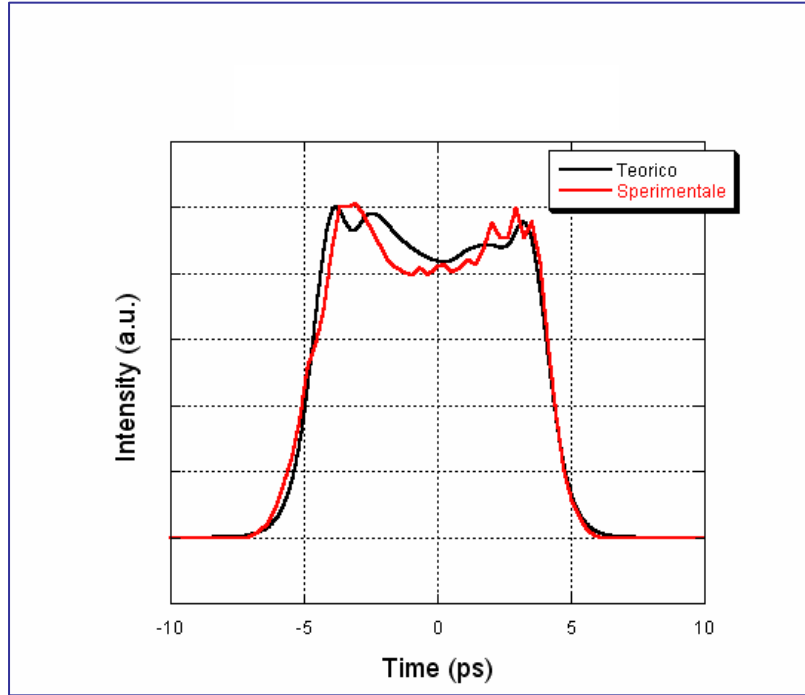

Fig. 9. Measured (red curve) and simulated (black plot) UV intensity profile out of the modified UV stretcher.

Numerical simulations indicate that to further reduce the rise time it is important to increase the spectral width of the UV pulse. This require a dedicated work to replace the non-linear crystal with thinner ones and focus the laser beam at the entrance of the third harmonic generator to maintain a reasonable efficiency of frequency tripling process.

4   ACKNOWLEDGMENTS

5   REFERENCES

[1]   J. Yang, F. Sakai, T. Yanagida, M. Yorozu, Y. Okada, K. Takasago, A. Endo, A. Yada, and M. Washio, J. Appl. Phys. **92**, 1608 (2002).

[2]   L. Palumbo and J. Rosenzweig, eds., *Technical Design Report for the SPARC Advanced Photo-Injector* (Laboratori Nazionali Frascati, Istituto Nazionale di Fisica Nucleare, 2004).

[3]   P. R. Bolton and J. E. Clendenin, Nucl. Instrum. Methods Phys. Res. A **483**, 296 (2002).

[4]   F. Verluise, V. Laude, J. P. Huignard, P. Tournois, and A. Migus, J. Opt. Soc. Am. B **17**, 138 (2000).

[5]   S. Cialdi, M. Petrarca, C. Vicario, Opt. Lett. Vol 31, (2006), 2885, and Virtual Journal of Ultrafast Science Oct. 2006.

[6]   S. Cialdi and I. Boscolo, Nucl. Instrum. Methods Phys. Res. A **538**, 1 (2005).

[7]   S. Cialdi, I. Boscolo, and F. Castelli, Appl. Phys. B **3**, 383 (2006).

[8]   A. Yariv, *Quantum Electronics*, 3rd ed. (Wiley, 1989).

[9]   E. Sidick, A. Knoesen, and A. Dienes, J. Opt. Soc. Am. B **12**, 1704 (1995).

[10]   M. Petrarca, C. Vicario, S. Cialdi, P. Musumeci, G. Gatti, A. Ghigo, and M. Mattioli, Rep. INFN-SPARC/LS-06/002 (INFN-SPARC, 2006).

[11]   S. Cialdi, C. Vicario, M. Petrarca, P. Musumeci Appl. Opt., Doc. ID 82759, (Posted 05/15/2007, in press).